J. Fluid Mech. (2009), *vol.* 619, *pp.* 147–166.
doi:10.1017/S0022112008004552 Printed in the United Kingdom

On the generation of lift forces in random soft porous media

P. MIRBOD, Y. ANDREOPOULOS AND S. WEINBAUM†

Departments of Biomedical and Mechanical Engineering, The City College of the City University of New York, New York, NY 10031, USA

(Received 8 April 2008 and in revised form 24 September 2008)

In this paper, we examine the generation of pressure and lift forces in a random soft fibrous media layer that is confined between two planar surfaces, an infinite horizontal lower boundary and a horizontal inclined upper boundary, in the lubrication limit where the characteristic thickness of the fibre layer $H \ll L$ the length of the inclined surface. The model for the fibre layer is a Brinkman equation and the Darcy permeability K_p is described by the widely used Carman–Kozeny equation for random porous media. Two cases are considered: (*a*) an inclined upper boundary which slides freely on top of a stationary fibre layer which is firmly attached to the lower boundary and (*b*) an inclined stationary upper boundary with an attached fibre layer in which the horizontal lower boundary slides freely in its own plane beneath it. Superficially, the problems appear equivalent to the classical problem for a slider bearing where the solutions for the pressure distribution and lift force are independent of which boundary is moving. In this problem there is an optimum compression ratio $k = h_1/h_2 = 2.2$, where h_1 and h_2 are the heights at the leading and trailing edges, for maximum lift force. However, this symmetry is lost if the intervening space is filled with a soft porous fibrous material since the Brinkman equation is not invariant under a transformation of coordinates in which the inherently unsteady problem in case (*a*) is transformed to a steady reference frame in which the inclined upper boundary is stationary and the horizontal boundary with the adhered fibre layer moves below it. Although in the steady reference frame case (*a*) now appears to resemble case (*b*), the solutions are strikingly different and depend critically on the value of the dimensionless fibre interaction layer thickness $\alpha = H/\sqrt{K_p}$. For $\alpha \ll 1$ the solutions for both cases approach the classical solution for a slider bearing. For $\alpha \gg 1$ we show, using asymptotic analysis that the solutions diverge dramatically. In case (*a*) the pressure and lift force increase as α^2 and asymptotically approach a limiting behaviour for large values of α, first predicted in Feng and Weinbaum (*J. Fluid Mech.*, vol. 422, 2000, p. 288), while in case (*b*) the pressure and lift force decay as α^{-2} since the inclined upper boundary is screened by the fibre layer and the amount of fluid dragged through the fluid gap decreases as α increases and vanishes for $\alpha \gg 1$. The solution in case (*a*), where the inclined upper boundary moves, is of particular interest since it reveals the potential to generate enormous lift forces using commercially available inexpensive soft porous materials provided the lateral leakage at the edge of the planform can be eliminated through the use of a channel with impermeable sidewalls as first proposed in the work by Wu, Andreopolous and Weinbaum (*Phys. Rev. Lett.*, vol. 93, 2004, p. 194501). The behaviour is illustrated for

† Email address for correspondence: weinbaum@ccny.cuny.edu

both a toboggan sliding in such a channel and a larger planform that might be useful in commercial transportation.

1. Introduction

In this paper, we examine the generation of pressure and lift forces in a random soft fibrous media layer that is confined between two planar surfaces, an infinite horizontal lower boundary and a horizontal inclined upper boundary, in the lubrication limit where the characteristic thickness of the fibre layer $H \ll L$ the length of the inclined surface. This type of flow has arisen in a number of important flow applications in which unexplained or unusual behaviour has either been observed or theoretically predicted. These include: (i) the anomalous behaviour observed in the single file motion of red cells *in vivo* and in small glass tubes of comparable diameter (Pries *et al.* 1994; Pries, Secomb & Gaehtgens 2000), (ii) the striking similarity between a red cell gliding on the endothelial glycocalyx (0.2–0.5 μm thick fibre matrix layer coating the inner lining of all our blood vessels) and a human being snow boarding on fresh snow powder (Feng and Weinbaum 2000; Wu *et al.* 2006) and (iii) the possibility of generating vastly enhanced lift forces using a novel track in which an inclined planar surface rides on a soft porous fibre layer in a channel with impermeable side walls (Wu, Andreopolous & Weinbaum 2004).

The studies in (i) describe a fundamental paradox that attracted considerable attention in the biorheology community in the 1980s and 1990s. Numerous experimental studies summarized in Pries *et al.* (1994, 2000) had clearly shown that the flow resistance of red cells moving single file in true capillaries had several times the resistance of red cells moving in narrow glass tubes of comparable diameter, reviewed in Chien, Usami & Skalak (1984). This was particularly evident in capillaries of 5–6 μm diameter where the 8 μm red cell underwent large deformations from its biconcave disc shape and assumed the shape of a moving bolus. Superficially, the flow problems appeared to be identical, but Vink and Duling (1996) demonstrated *in vivo* that the inner lining of our capillaries was lined with a ubiquitous endothelial glycocalyx layer of 0.4–0.5 μm thickness. The properties of this layer and its various functions have recently been reviewed in Weinbaum, Tarbell & Damiano (2007). One of the most striking observations in Vink and Duling was the so-called 'popout' phenomenon in which a red cell starting from rest would rise out of the layer as its velocity increased and at a velocity greater than $20\,\mu\mathrm{m\,s^{-1}}$ enter the central lumen of the vessel where upon it would move above the glycocalyx edge on a thin lubricating film. This was explained in Feng and Weinbaum (2000), using a lubrication theory for soft porous media in which the authors predicted that greatly enhanced lift forces could be produced in the glycocalyx layer at velocities less than $20\,\mu\mathrm{m\,s^{-1}}$ due to the large increase in pressure in the trapped porous layer between the red cell and the endothelial cell membranes. Detailed calculations in Secomb, Hsu & Pries (2001) clearly confirmed this prediction for a flexible red cell moving axisymmetrically along the axis of a cylindrical tube lined with a compressible matrix layer satisfying the Brinkman equation. In marked contrast, red cells in glass tubes appear to fill nearly the entire lumen of the tube when moving at both high and low speeds suggesting that if there was an adhered layer of macromolecules coating the red cell membrane these lift forces were either absent or greatly diminished.

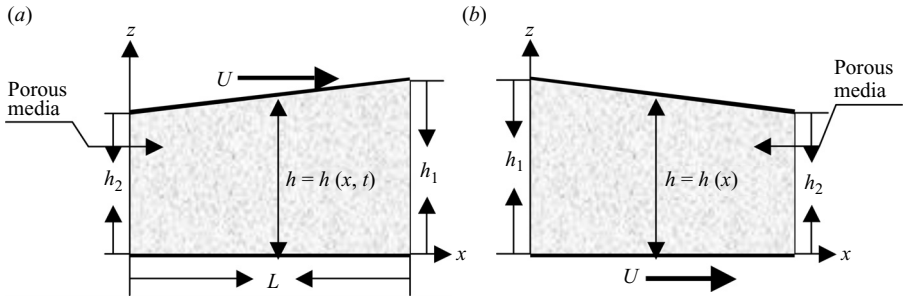

FIGURE 1. Schematic illustration of the present model for sliding motion of a rigid surface over or beneath a thin layer of a soft fibre matrix. (*a*) Inclined planar surface moves over a stationary matrix attached to the lower boundary. (*b*) Horizontal planar surface moves beneath a stationary matrix attached to the inclined upper boundary.

The red cells moving in narrow glass tubes and in capillaries illustrate the two superficially similar flow geometries that will be examined in this paper. In the case of the red cells moving in capillaries (figure 1*a*), a planing surface is moving with a small tilt angle relative to a horizontal rigid boundary with an attached matrix layer. This is an inherently unsteady problem in which the lower boundary and its attached fibre layer are stationary and the latter is being compressed by the tilt of the moving upper boundary which drives the fluid through the attached porous layer. The theories of Weinbaum *et al.* (2003) and Han *et al.* (2006) show that if the fibres have a flexural rigidity EI of $\sim$500 pN nm^2, this would be sufficient to prevent any significant change in thickness of the glycocalyx layer when it is exposed to fluid shear stresses in the physiological range at its top surface. However, this flexural rigidity would be insufficient to prevent the layer from collapsing when the motion of the red cell is arrested. Weinbaum *et al.* propose that the major function of the small flexural rigidity of the glycocalyx fibres is the transmission of fluid shear stresses to the internal actin cytoskeleton of the cell in mechanotransduction. This was clearly demonstrated in Thi *et al.* (2004) where cytoskeletal responses were abrogated when the glycocalyx was enzymatically compromised. The resistance to compression of the glycocalyx has also been attributed to oncotic forces arising from trapped proteins in the layer (Secomb, Hsu & Pries 2001) or electro-chemical repulsive forces (Damiano and Stace 2002). In the case of red cells moving in glass tubes, where a matrix layer is also believed to be attached to the red cell membrane (figure 1*b*), one has a steady problem. Here both the red cell and its attached matrix layer are stationary and the horizontal lower boundary moves beneath it without any compression of the matrix.

The mechanical properties of the glycocalyx have been largely deduced from the nonlinear elastic recoil of the glycocalyx layer after the passage of a tightly fitting white cell. This recoil is described using large deformation 'elastica' theory for the fibres and a Brinkman equation for the fluid motion in Han *et al.* (2006). A more general small deformation theory for the deformation of the fibres when subject to oscillating fluid shear stress is presented in Han, Ganatos & Weinbaum (2005). In the present analysis the shear deformation of the fibres is neglected but the variation in permeability K_p due to the local compression of the layer is considered. It is assumed that the fibres compress easily and contribute negligibly to the lift forces exerted on the inclined upper boundary. In the absence of this elastic restoring force there is little friction between the fibres and inclined upper boundary. Similarly, for

the soft fibre-fill used in the applications given in § 6 one observes only minor shear deformations of the matrix.

The enhanced pressure and lift forces generated in the matrix by the motion of the inclined upper boundary in figure 1(*a*) was first treated in Feng & Weinbaum (2000), who developed a two-dimensional generalized lubrication theory for highly compressible porous media using effective medium theory based on the use of the Brinkman equation. Prior analyses by Damiano (1998) and Secomb, Hsu & Pries (1998) also used a Brinkman equation to describe the flow in the glycocalyx layer, but the red cells did not invade the layer and a thin layer of fluid was assumed to exist between the edge of the layer and the red cell membrane. In Feng & Weinbaum (2000) the authors also treat the Darcy permeability parameter $\alpha = H/\sqrt{K_p}$ as a spatially varying parameter that takes account of the local elastic compression of the fibres. The two most striking predictions of this analysis were that (i) greatly enhanced lift forces could be generated that scaled as α^2 for large α as the compression of the fibre matrix increased and (ii) as unexpected as it might seem at first glance, the value of α for a red cell gliding on the glycocalyx layer, which was estimated as 160, was nearly the same as a human snowboarding on fresh snow powder, although the red cell and human differ in mass by 15 orders of magnitude. In this initial study the Darcy permeability K_p was computed for a deformed periodic array of parallel cylindrical fibres using an extension of the theory of Sangani and Acrivos (1982) for Stokes flow transverse to the fibre array.

One of the unexpected predictions of the analysis in Feng & Weinbaum (2000) was that, there was no optimum compression ratio, $k = h_1/h_2$, where the lift force could be maximized when h_1 is fixed. Here the subscripts 1 and 2 refer to the leading and trailing edges, respectively, of the planar surface. In marked contrast, for classical lubrication theory, $\alpha = 0$ (no fibres present), one of the best known results for a slider bearing is that for $k = 2.2$, one obtains maximum lift when the height of the trailing edge h_2 is held fixed. Another well-known result of classical lubrication theory for the slider bearing is that the pressure distribution in the fluid gap is identical whether the inclined upper boundary or the flat lower boundary is moving. This does not hold true when the intervening layer is a confined porous media where a dramatic difference in behaviour emerges as α increases for $\alpha > 1$ depending on whether the matrix is attached to the horizontal lower or inclined upper boundary. We shall show herein that the pressure distribution decays to zero in case (*b*) where the lower boundary moves and the inclined boundary and matrix are stationary, whereas in case (*a*) where the inclined upper boundary moves and the lower boundary and matrix are stationary, one obtains the huge increase in lift described in Feng & Weinbaum (2000) as α increases. These paradoxical behaviours are analysed in the present paper both numerically and using asymptotic analysis for small and large values of α.

Subsequent to Feng & Weinbaum (2000), Wu *et al.* (2005) theoretically and experimentally explored the large α behaviour for snow using a novel piston-porous cylinder apparatus where the escape of air from the compressed snow layer was examined on the time scale of skiing or snowboarding for the first time. These results were then used to develop a more general theory for skiing and snowboarding wherein the forces and moments due to both the trapped air and the compressed solid phase of the ice crystals were taken into account and empirically determined values of the Darcy permeability of snow were employed for different snow conditions (Wu *et al.* 2006). However, in either skiing or snowboarding there is a large loss of pore pressure at the lateral edges of the ski or snowboard and the pressure and lift force decrease as $(W/L)^2$ for large α where W is the width of the planing surface. This observation

led the authors in Wu *et al.* (2004) to propose a novel soft porous track wherein the fibre layer is attached to the bottom boundary of a channel with impermeable sidewalls. This would enable one to exploit the full effect of the huge increase in lift for $\alpha \gg 1$ by eliminating the loss of pressure at the lateral edges. For this case, the two-dimensional analysis in Feng & Weinbaum (2000) for a ski or snowboard reduces to the much simpler unidirectional flow geometry in figure 1(*a*). Wu *et al.* (2004) also show that this new track had the potential to support the weight of a train car moving at relatively modest speeds on synthetic porous materials, which had the permeability properties of down feathers. This prediction led to a search for a soft durable inexpensive porous material with similar permeability properties and the discovery that the polyester fibres used in inexpensive body pillows were ideal for this application (Mirbod, Andreopoulos & Weinbaum in press). This fibre-fill material is more adequately described by the widely used empirical Carman–Kozeny equation for random porous media. The calculations in the present study are performed using this empirical relation and the results applied to both a toboggan riding on a soft porous track and a jet train that is described in much greater detail in Mirbod *et al.* (in press).

In F&W and all previous studies of the glycocalyx layer, the flow in the matrix has been described using a Brinkman equation. As pointed out by the reviewers, the Darcy term in the Brinkman equation is not frame invariant under a Galilean transformation in which the flow geometry in case (*a*) (figure 1*a*) is transformed to a steady coordinate system in which the observer rides on the inclined upper boundary and the lower boundary with its attached matrix moves with uniform velocity U to the left. Although cases (*a*) and (*b*) now look similar, they differ as the matrix is attached (*a*) to the lower boundary and (*b*) to the upper boundary. This difference leads to a new α^2 term in the generalized dimensionless Brinkman equation which is related to the flow that is generated by the tilt of the moving upper boundary in the original unsteady coordinate system in figure 1(*a*). This generalized equation, which is based on binary mixture theory for a dilute solid constituent takes account of the relative motion of the fluid and solid phases in the description of the Darcy term (Roy & Damiano 2008). The pressure and lift force are unaffected since they are independent of the velocity transformation.

The paper is organized into six sections. In § 2, the governing equations for cases (*a*) and (*b*) are derived. In § 3, we examine the behaviour of the Carman–Kozeny equation for a random array of cylindrical fibres of uniform radius. In § 4, we numerically solve the governing equations for cases (*a*) and (*b*) and perform an asymptotic analysis for small and large values of α for both flow geometries. In § 5, we present the results, and in § 6 we briefly describe the applications.

2. Lubrication theory for the fibrous layer

Classical lubrication theory was initially developed by Reynolds for an incompressible Newtonian fluid (Schlichting 1979). This was subsequently generalized for Newtonian fluids with variable properties and non-Newtonian fluids. The theory has been applied to both impermeable and porous walled journal-bearing systems. A more recent application of lubrication theory has been to biological systems where the walls are not porous, but the lubricating layer itself is a soft porous medium. As first proposed by Damiano (1998) and Secomb *et al.* (1998), this layer has been described by a Brinkman equation (Brinkman 1947) in nearly all subsequent theoretical analyses. Shortly thereafter, Feng & Weinbaum (2000) demonstrated that if the red cell entered the glycocalyx layer its compression could be large leading to significant variations in

the Darcy permeability K_p and dramatic changes in the pressure distribution in the layer for large compressions.

The inherently unsteady-flow problem in figure 1(*a*) can be readily converted to a steady flow in which a fix observer sits on the inclined upper boundary and the lower boundary with its attached matrix moves with velocity $\bar{\boldsymbol{u}}_s = -U\boldsymbol{i}$ to the left beneath it. In this new steady (x', z') coordinate system the absolute velocity of the fluid in the x'-direction is $\bar{\boldsymbol{u}} = u'\boldsymbol{i}$ and the relative velocity between the fluid and solid constituents which appears in the Darcy term is $\bar{\boldsymbol{u}} - \bar{\boldsymbol{u}}_s = (u' + U)\boldsymbol{i}$. The generalized Brinkman equation for the motion of the fluid in the steady coordinate system is given by Roy and Damiano (2008) as

$$\frac{\partial^2 u'}{\partial z'^2} - \frac{u' + U}{K_p} = \frac{1}{\mu}\frac{\mathrm{d}p'}{\mathrm{d}x'}. \tag{2.1}$$

Here μ is the fluid viscosity, p' is the fluid pressure and primes indicate dimensional quantities. Equation (2.1) can be written in dimensionless form by introducing the dimensionless quantities

$$x = \frac{x'}{L}, \quad z = \frac{z'}{h'}, \quad h = \frac{h'}{H}, \quad p = \frac{p'H^2}{\mu LU}, \quad u = \frac{u'}{U}. \tag{2.2}$$

Here L is the length of the planing surface, $h(x,t)$ is a local dimensionless height scaled by H a convenient reference height and U is the magnitude of the velocity of the lower boundary and solid phase. The dimensionless form of (2.1) is

$$\frac{\partial^2 u}{\partial z^2} - \alpha^2(u + 1) = \frac{\mathrm{d}p}{\mathrm{d}x}. \tag{2.3}$$

The solution to (2.3) which satisfies the no-slip boundary conditions $u(x, 0) = -1$ at $z = 0$ and $u(x, h) = 0$ at $z = h$ is given by

$$u(x, z) = \frac{\sinh \alpha z}{\sinh \alpha h} + \frac{1}{\alpha^2}\frac{\partial p}{\partial x}\left[\cosh \alpha z - 1 - \frac{\sinh \alpha z}{\sinh \alpha h}(\cosh \alpha h - 1)\right] - 1. \tag{2.4}$$

The corresponding flux in the x-direction is computed by integrating over the local dimensionless channel height

$$Q = \int_0^h u\mathrm{d}z = f + \frac{1}{\alpha^2}\frac{\partial p}{\partial x}(2f - h) - h, \tag{2.5}$$

where,

$$f = \frac{\cosh \alpha h - 1}{\alpha \sinh \alpha h}, \quad \alpha = \frac{H}{\sqrt{K_p}}. \tag{2.6}$$

Here α is a dimensionless permeability parameter defined in terms of K_p the dimensional Darcy permeability. In the transformed steady coordinate system the flux Q is a constant from continuity and thus,

$$\frac{\mathrm{d}Q}{\mathrm{d}x} = 0. \tag{2.7}$$

Combining (2.5) and (2.7) one has,

$$\frac{\partial}{\partial x}\left[f + \frac{1}{\alpha^2}\frac{\mathrm{d}p}{\mathrm{d}x}(2f - h)\right] = \frac{\mathrm{d}h}{\mathrm{d}x}. \tag{2.8}$$

This last result is the same as (2.25) in Feng & Weinbaum (2000), which was derived without using this coordinate transformation. The results for the velocity profiles and streamlines are also plotted in the moving unsteady coordinate system in Feng & Weinbaum (2000). The pressure profiles and lift forces are independent of coordinate system.

For case (*b*) (figure 1*b*) there is no need to transform coordinates since the matrix is attached to the stationary inclined upper boundary and the horizontal lower boundary moves in its own plane to the right. Thus $\bar{\boldsymbol{u}}_s = 0$, the α^2 term in (2.3) is missing, and the second term reduces to $-\alpha^2 U$. There is no compression of the porous media as in case (*a*). The solution of (2.3) with the α^2 term missing which satisfies the no-slip boundary conditions $u(x, 0) = +1$ at $z = 0$ and $u(x, h) = 0$ at $z = h$ is given by

$$u(x,z) = -\cosh\alpha h \frac{\sinh\alpha z}{\sinh\alpha h} + \cosh\alpha z + \frac{1}{\alpha^2}\frac{\partial p}{\partial x}\left[\cosh\alpha z - 1 - \frac{\sinh\alpha z}{\sinh\alpha h}(\cosh\alpha h - 1)\right]. \tag{2.9}$$

The corresponding flux in the x-direction is given by

$$Q = \int_0^h u\,\mathrm{d}z = f + \frac{1}{\alpha^2}\frac{\partial p}{\partial x}(2f - h). \tag{2.10}$$

Again continuity requires that Q is constant or

$$\frac{\mathrm{d}Q}{\mathrm{d}x} = 0. \tag{2.11}$$

Combining (2.10) and (2.11), in case (*b*) one has,

$$\frac{\partial}{\partial x}\left[f + \frac{1}{\alpha^2}\frac{\mathrm{d}p}{\mathrm{d}x}(2f - h)\right] = 0. \tag{2.12}$$

In cases (*a*) and (*b*) h_2 is fixed and chosen as the reference height H. The term on the right-hand side of (2.8) is due to the forward motion of the upper inclined plane in figure 1(*a*), which compresses the stationary matrix layer, whereas this term vanishes in (2.12) because the inclined upper boundary and its attached matrix are stationary. In classical lubrication theory it does not make any difference which plane is moving since the starting momentum equation without the second term on the left-hand side of (2.1) is invariant under a Galilean coordinate transformation.

The Reynolds equations (2.8) and (2.12) can be solved for the pressure distribution using appropriate boundary conditions. Once the pressure field is determined, the velocity profiles and the lift force are readily obtained. These results are presented and discussed in §§ 4 and 5.

3. Permeability of the fibrous media

In F&W the variation of K_p with x is determined by solving the Stokes creeping motion equations for the flow perpendicular to the axis of an array of circular cylindrical fibres whose vertical spacing changes proportionally with the local dimensionless height h. In the present application we shall consider a random array of cylindrical fibres of uniform diameter. This is a very good representation for the inexpensive polyester fibre-fill that is extensively used in commercially available pillows. This material has been chosen because of the applications that are discussed in § 6. A random fibre array of this nature is most conveniently described by the

widely used empirical Carman–Kozeny equation (see Happel and Brenner 1983)

$$K_p = \frac{\varepsilon^3}{G s_0^2 (1-\varepsilon)^2}, \tag{3.1}$$

where ε is the void fraction, $(1-\varepsilon)$ is the solid fraction, G is the empirically measured Kozeny constant and s_0 is the Carman-specific surface, defined as the area of the surface that is exposed to the fluid per unit volume of the solid phase. For cylindrical fibres of radius r_f

$$s_0 = \frac{2\pi r_f L_f}{\pi r_f^2 L_f} = \frac{2}{r_f}, \tag{3.2}$$

where L_f is the total fibre length per unit volume. For these fibres, (3.1) becomes

$$K_p = \frac{r_f^2 \varepsilon^3}{4G(1-\varepsilon)^2}. \tag{3.3}$$

The value of G depends on the porosity. When the fibres are randomly oriented, Happel and Brenner (1983) give the following expression for $G(\varepsilon)$:

$$G(\varepsilon) = \frac{2\varepsilon^3}{3(1-\varepsilon)} \left\{ \frac{1}{-2\ln(1-\varepsilon) - 3 + 4(1-\varepsilon) - (1-\varepsilon)^2} + \frac{2}{-\ln(1-\varepsilon) - [1-(1-\varepsilon)^2]/[1+(1-\varepsilon)^2]} \right\}. \tag{3.4a}$$

When $\varepsilon \to 1$, (3.4a) is frequently approximated by (Truskey, Yuan & Katz, 2004)

$$G(\varepsilon) \to \frac{-5}{3(1-\varepsilon)\ln(1-\varepsilon)}. \tag{3.4b}$$

One observes from (3.3) that K_p/r_f^2 is only a function of $(1-\varepsilon)$ for both (3.4a) and (3.4b) when $\varepsilon \to 1$. Since $(1-\varepsilon)$ will be less than 0.01 for all values of α considered herein, one concludes from figure 2 that K_p/r_f^2 is closely approximated by

$$\frac{K_p}{r_f^2} = -\frac{3}{20}\frac{\ln(1-\varepsilon)}{(1-\varepsilon)}, \tag{3.5}$$

obtained by combining (3.3) and (3.4b).

The variation of K_p/r_f^2 as a function of h/h_2 is obtained directly from the curves in figure 2. A relatively simple and reasonable assumption is that when the fibre layer is compressed the increase in fibre density is locally proportional to the decrease in height of the fibre layer as a function of x. Thus, the solid fraction $(1-\varepsilon)$ decreases as h_2/h where h_2 is the height of the layer at the leading edge of the planform in case (b) and the trailing edge in case (a). Using (3.5) and the foregoing assumptions for the variation of K_p with h, one can define a dimensionless local Darcy permeability $\tilde{K}_p$ by

$$\tilde{K}_p = \frac{K_p(h)}{K_{p2}} = h - \frac{h\ln h}{\ln(1-\varepsilon_2)}, \tag{3.6}$$

where K_{p_2} is the minimum value at $h = h_2$. Figure 3 shows the variation of $K_p(h)/K_{p2}$ as a function of h/h_2 for representative values of $(1-\varepsilon_2)$ in which ε_2 is the void fraction at $h = h_2$. The value of $(1-\varepsilon)$ for the polyester fibre-fill in the undeformed state in our applications in § 6 is 0.00467.

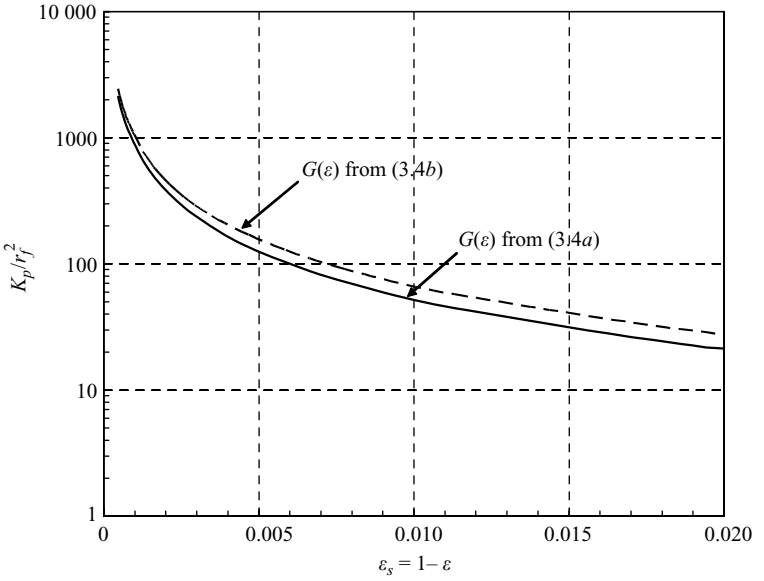

FIGURE 2. Comparison of K_p/r_f^2 using (3.4*a*) and (3.4*b*) for the Carman–Kozeny constant $G(\varepsilon)$.

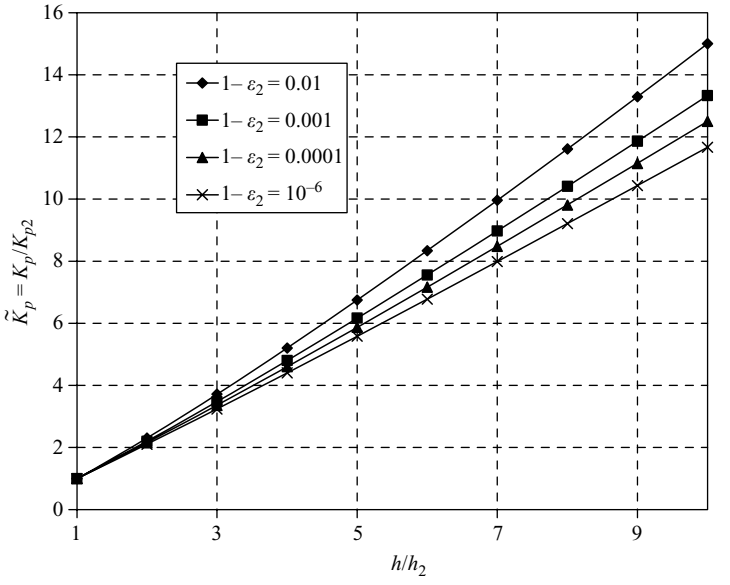

FIGURE 3. Variation of $\tilde{K}_p = K_p/K_{p2}$ as a function of h/h_2 for representative values of $(1-\varepsilon_2)$.

4. Solutions to boundary value problem

A general solution to the boundary value problem for (2.8) and (2.12) can be obtained by applying boundary conditions at the leading and trailing edges of the planform, $x = 0$ and 1. This general solution was previously obtained for case (*a*), inclined upper boundary moving, in Feng & Weinbaum (2000), but is included herein for easy comparison with case (*b*), which is new. We will then examine the behaviour

of these solutions for both $\alpha \ll 1$ and $\alpha \gg 1$. In the small α limit it is clear that cases (a) and (b) are identical for $\alpha = 0$, but differ by the α^2 term in (2.3) for $\alpha > 0$. We shall use perturbation theory to calculate the lowest order corrections for the pressure distribution in the two cases. In the large α limit the two solutions dramatically diverge, one solution for pressure and lift force increasing as α^2 and the other decaying as α^{-2}.

The general solutions to (2.8) and (2.12) can be obtained for an arbitrary variation of $h(x)$ assuming that K_p, and hence α, only vary with x. Note also that the tilt of the inclined boundary has been reversed for the two cases so that the pressure profiles will not lie on top of one another in the small α limit. As discussed in the previous section the compression of the fibre layer is assumed to be locally uniform throughout the height of the layer. The first integrals of (2.8) and (2.12) are

$$f + \frac{1}{\alpha^2}\frac{\mathrm{d}p}{\mathrm{d}x}(2f - h) = h + C_1, \tag{4.1a}$$

$$f + \frac{1}{\alpha^2}\frac{\mathrm{d}p}{\mathrm{d}x}(2f - h) = C_2, \tag{4.1b}$$

where C_i, $i = 1, 2$, are constants of integration. The constants C_i are evaluated by prescribing the leading and trailing edge pressures. The C_i can be expressed as

$$C_1 = -\frac{\displaystyle\int_0^1 \alpha^2(h - f)/(2f - h)\,\mathrm{d}x}{\displaystyle\int_0^1 \alpha^2/(2f - h)\,\mathrm{d}x}, \tag{4.2a}$$

$$C_2 = \frac{\displaystyle\int_0^1 \alpha^2 f/(2f - h)\,\mathrm{d}x}{\displaystyle\int_0^1 \alpha^2/(2f - h)\,\mathrm{d}x}. \tag{4.2b}$$

The pressure distributions from (4.1a) and (4.1b) are given by

$$p_1(x) - p_0 = \int_0^x \frac{\alpha^2(h + C_1 - f)}{2f - h}\,\mathrm{d}x, \tag{4.3a}$$

$$p_2(x) - p_0 = \int_0^x \frac{\alpha^2(C_2 - f)}{2f - h}\,\mathrm{d}x, \tag{4.3b}$$

in which p_0 is the atmospheric pressure at $x = 0$ and 1 and the C_i are given by (4.2a) and (4.2b). The total dimensionless lift force F is obtained by integrating (4.3a) and (4.3b) over the entire surface. This leads to

$$F_1 = \int_0^1 (p_1(x) - p_0)\,\mathrm{d}x = \int_0^1 (1 - x)\frac{\alpha^2(h + C_1 - f)}{2f - h}\,\mathrm{d}x, \tag{4.4a}$$

$$F_2 = \int_0^1 (p_2(x) - p_0)\,\mathrm{d}x = \int_0^1 (1 - x)\frac{\alpha^2(C_2 - f)}{2f - h}\,\mathrm{d}x, \tag{4.4b}$$

where we have changed the order of integration in evaluating the double integral. Once $h(x)$ is prescribed, (4.2)–(4.4) provide a remarkably simple solution for the pressure distribution and lift force in the compressed matrix layer for any $h(x)$.

4.1. *Small α limit*

In the limit $\alpha \to 0$, one can expand f in (2.6) as

$$f \to \frac{h}{2} - \frac{\alpha^2 h^3}{24} + \frac{\alpha^4 h^5}{240} + O(\alpha^6). \tag{4.5}$$

If one substitutes the first two terms of (4.5) into (4.2*a*, *b*) and retains only the terms which are order $O(1)$, one finds that $C_1 = -C_2$ (see (4.8*a*, *b*). If these values of the C_i are now put back in (4.1*a*, *b*) one obtains

$$\frac{\mathrm{d}p}{\mathrm{d}x} = \pm\frac{12C_1}{h^3} \pm \frac{6}{h^2}, \tag{4.6}$$

where the minus sign describes case (*a*) and the plus sign describes case (*b*). Thus, in the limit $\alpha = 0$ the two cases are identical except that the pressure gradient at x in case (*a*) is the negative of the pressure gradient at $(1 - x)$ in case (*b*), as noted previously. This is simply a result of the fact that the slopes of the upper boundaries in figure 1(*a*, *b*) are reversed and when (4.6) is integrated the pressure profiles will be mirror images of one another.

The above symmetry is lost once one retains the third term in (4.5). The common expression $\alpha^2/(2f - h)$ that appears in (4.2) and (4.3) can be expanded as

$$\frac{\alpha^2}{2f - h} = -\frac{12}{h^3}\left(1 + \frac{\alpha^2 h^2}{10} + O(\alpha^4)\right). \tag{4.7}$$

To $O(\alpha^2)$ one finds from (4.2*a*, *b*) that C_1 and C_2 are

$$C_1 = -\frac{\displaystyle\int_0^1 (1/h^2)\,\mathrm{d}x}{2\displaystyle\int_0^1 (1/h^3)\,\mathrm{d}x} - \frac{\alpha^2}{20\displaystyle\int_0^1 (1/h^3)\,\mathrm{d}x}\left[\frac{11}{6} - \frac{\displaystyle\int_0^1 (1/h^2)\,\mathrm{d}x \int_0^1 (1/h)\,\mathrm{d}x}{\displaystyle\int_0^1 (1/h^3)\,\mathrm{d}x}\right] + O(\alpha^4), \tag{4.8a}$$

$$C_2 = \frac{\displaystyle\int_0^1 (1/h^2)\,\mathrm{d}x}{2\displaystyle\int_0^1 (1/h^3)\,\mathrm{d}x} + \frac{\alpha^2}{20\displaystyle\int_0^1 (1/h^3)\,\mathrm{d}x}\left[\frac{1}{6} - \frac{\displaystyle\int_0^1 (1/h^2)\,\mathrm{d}x \int_0^1 (1/h)\,\mathrm{d}x}{\displaystyle\int_0^1 (1/h^3)\,\mathrm{d}x}\right] + O(\alpha^4). \tag{4.8b}$$

Using (4.5) and (4.6) and simplifying, one obtains

$$p_1 - p_0 = -\int_0^x \frac{6}{h^2}\,\mathrm{d}x - \int_0^x \frac{12C_1}{h^3}\,\mathrm{d}x - \frac{\alpha^2}{10}\left[\int_0^x \frac{12C_1}{h}\,\mathrm{d}x + 11x\right] + O(\alpha^4), \tag{4.9a}$$

$$p_2 - p_0 = \int_0^x \frac{6}{h^2}\,\mathrm{d}x - \int_0^x \frac{12C_2}{h^3}\,\mathrm{d}x - \frac{\alpha^2}{10}\left[\int_0^x \frac{12C_2}{h}\,\mathrm{d}x - x\right] + O(\alpha^4). \tag{4.9b}$$

One can readily show that the term in α^2 is positive for case (*a*) and negative for case (*b*) indicating that the presence of the fibres increases the pressure in case (*a*) but decreases it in case (*b*). The total dimensionless lift force F is obtained by integrating

(4.9*a*) and (4.9*b*) over the entire surface.

$$F_1 = \int_0^1 (p_1 - p_0)\,\mathrm{d}x = -\int_0^1 (1-x)\left[\frac{6}{h^2} + \frac{12C_1}{h^3} + \left(\frac{12C_1}{10h} + \frac{11}{10}\right)\alpha^2 + O(\alpha^4)\right]\mathrm{d}x, \tag{4.10a}$$

$$F_2 = \int_0^1 (p_2 - p_0)\,\mathrm{d}x = \int_0^1 (1-x)\left[\frac{6}{h^2} - \frac{12C_2}{h^3} - \left(\frac{12C_2}{10h} - \frac{1}{10}\right)\alpha^2 + O(\alpha^4)\right]\mathrm{d}x. \tag{4.10b}$$

These results provide the lowest order correction to $O(\alpha^2)$ for cases (*a*) and (*b*) that arise from the difference between (2.8) and (2.12).

4.2. *Large α limit*

To examine the asymptotic behaviour of the pressure distribution in the soft porous layer when $\alpha \gg 1$, we notice from (2.8) that, in this limit, $f \approx \alpha^{-1}$. If we consider case (*a*), we find that (4.2*a*) and (4.3*a*) reduce to

$$C_1 = -\frac{\displaystyle\int_0^1 (1/\tilde{K}_p)\,\mathrm{d}x}{\displaystyle\int_0^1 (1/h\tilde{K}_p)\,\mathrm{d}x}, \tag{4.11a}$$

$$p_1 - p_0 \approx -\alpha_2^2 \int_0^x \frac{(h + C_1)}{\tilde{K}_p h}\,\mathrm{d}x. \tag{4.12a}$$

If we consider case (*b*), we find that (4.2*b*) and (4.3*b*) reduce to

$$C_2 = \frac{\displaystyle\int_0^1 (1/h\sqrt{\tilde{K}_p})\,\mathrm{d}x}{\alpha_2 \displaystyle\int_0^1 (1/h\tilde{K}_p)\,\mathrm{d}x}, \tag{4.11b}$$

$$p_2 - p_0 \approx -\alpha_2 \int_0^x \left(\frac{-\alpha_2 C_2}{\tilde{K}_p h} + \frac{1}{h\sqrt{\tilde{K}_p}}\right)\mathrm{d}x. \tag{4.12b}$$

In (4.11) and (4.12) we have rewritten α in a form where we can scale this spatially varying parameter by its reference value α_2 at $h = h_2$. This scaling will permit us to relate both α and K_p to their reference values at $h = h_2$ in plotting our results as described in the opening paragraph of the next section. Using (3.6) one can convert the integrals on x in (4.11) and (4.12) to integrals on h that are much easier to evaluate. For case (*a*)

$$C_1 = -\frac{\ln\left(1 - \ln(k)/\ln(1-\varepsilon_2)\right)}{\mathrm{e}^{-\ln(1-\varepsilon_2)}\left[Ei\left[\ln(1-\varepsilon_2)/k\right] - Ei\left[\ln(1-\varepsilon_2)\right]\right]} \tag{4.13a}$$

in which

$$Ei(x) = -\int_{-x}^{\infty} \frac{\mathrm{e}^{-t}}{t}\,\mathrm{d}t,$$

and

$$p_1 - p_0 \approx -\alpha_2^2 \int_1^h \frac{h + C_1}{h^2(1 - \ln h/\ln(1-\varepsilon_2))}\,\mathrm{d}h, \tag{4.14a}$$

whereas for case (*b*)

$$C_2 = \frac{\int_k^1 (1/h^{3/2}\sqrt{1 - \ln h/\ln(1-\varepsilon_2)})\,\mathrm{d}h}{\int_k^1 (\alpha_2/h^2(1 - \ln h/\ln(1-\varepsilon_2)))\,\mathrm{d}h}, \tag{4.13b}$$

and

$$p_2 - p_0 \approx -\alpha_2^2 \int_k^h \frac{C_2\,\mathrm{d}h}{h^2(1-k)(1-\ln h/\ln(1-\varepsilon_2))} + \alpha_2 \int_k^h \frac{\mathrm{d}h}{h^{3/2}(1-k)\sqrt{1-\ln h/\ln(1-\varepsilon_2)}}. \tag{4.14b}$$

In case (*a*) the above results are particularly useful for large α where p can be scaled by α_2^2 and the pressure profiles collapse into a single curve for a given h_2 for each value of the compression ratio k as deduced from (4.14*a*). In case (*b*) for $\alpha_2 \gg 1$ the pressure asymptotically decays to zero as α_2^{-2}. These results are shown and discussed in the next section.

5. Results

We shall explore the behaviour of cases (*a*) and (*b*) over a wide range of α_2 and compression ratio $k = h_1/h_2$. The length L of the planing surface does not appear explicitly, but appears in the dimensionless expressions for the pressure and force per unit width of planing surface. The characteristic pressure and lift force F per unit width are given by $\mu UL/h_2^2$ and $\mu UL^2/h_2^2$, respectively. The dimensionless height h is scaled by the height h_2 at the trailing edge in case (*a*) and the leading edge in case (*b*). If h_2 is arbitrarily fixed at 1 cm then a reference α_2 can be defined by $h_2/\sqrt{K_{p2}}$ where K_{p2} is the reference Darcy permeability at this reference height. For $h > 1$, α varies with x since both h and K_p are varying, but $\tilde{K}_p$ is only a function of h for each value of k as shown in figure 3. Thus, to employ the results shown in figure 3 one simply specifies α_2, prescribes the fibre radius and finds K_{p2} from figure 2. The fibre radius r_f used in all our calculations is 5 μm. This is characteristic of the polyester fibres used in the applications in § 6.

In classical lubrication theory for a slipper bearing one examines the relative motion of an inclined planar surface and a horizontal planar surface. Figure 4(*a*, *b*) shows that the solution for the pressure distribution and lift force are independent of the boundary which is moving, for reasons already discussed, and there is an optimum compression ratio $k = h_1/h_2 = 2.2$ for maximum lift. As already noted, the solution for the pressure distribution in case (*a*) is the mirror image of that in case (*b*) because the inclination of the upper boundary is reversed. This symmetry is lost if the intervening space is filled with a soft porous material.

Typical solutions for the pressure distribution beneath the planar surface when the upper boundary moves (case *a*) and when the lower boundary moves (case *b*) are shown in figures 5(*a*) and 5(*b*) for a compression ratio $k = 2$ for values of α_2 in the range of $0 < \alpha_2 < 3$. In figure 5(*a*) the thickness h_2 and α_2 at the trailing edge are prescribed. The slope of the plane $(h_1 - h_2)/L$ is given in terms of the matrix compression ratio $k = h_1/h_2$ as $(k-1)h_2/L$ (see figure 1*a*). In figure 5(*b*) the thickness h_2 and α_2 at the leading edge are prescribed. The slope of the plane $-(h_1 - h_2)/L$ is given in terms of the matrix compression ratio $k = h_1/h_2$ as $(1-k)h_2/L$ (see figure 1*b*).

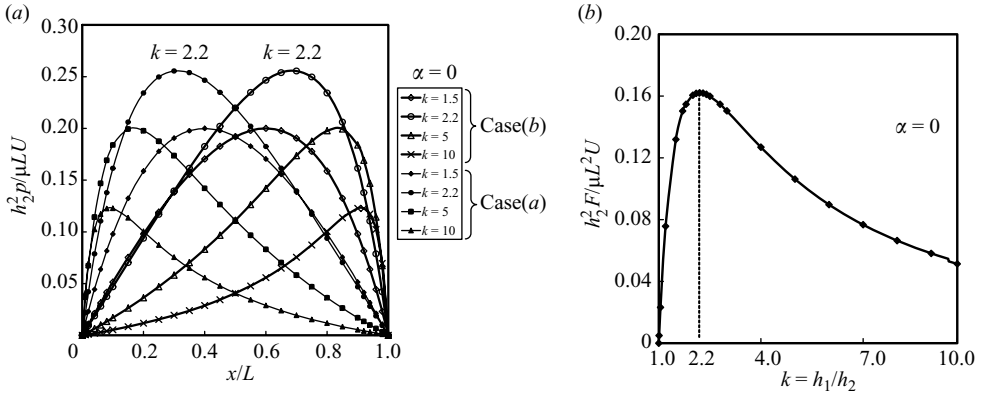

FIGURE 4. Classical lubrication theory $\alpha = 0$. (*a*) Dimensionless pressure distribution for a slipper bearing. (*b*) Dimensionless lift force as a function of compression ratio k showing a maximum at $k = 2.2$.

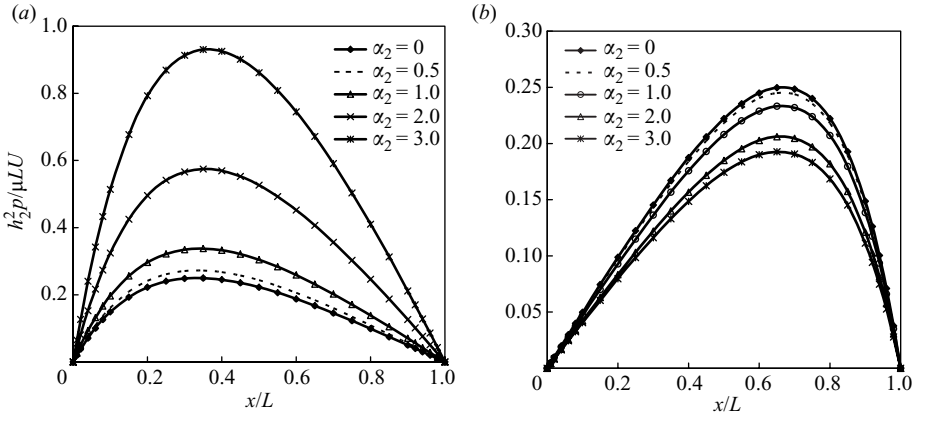

FIGURE 5. Dimensionless pressure distribution for compression ratio $k = 2$. (*a*) Inclined upper boundary moves. (*b*) Horizontal lower boundary moves. Dashed line solution for small α, (4.9*a*) in case (*a*), (4.9*b*) in case (*b*).

As can be seen in figure 5(*a*) when the inclined upper boundary moves the dimensionless pressure increases rapidly for $\alpha_2 > 1$ with the peak value of pressure being more than four-fold greater for $\alpha_2 = 3$ than for $\alpha = 0$. In contrast, when the horizontal lower boundary moves, the pressure profiles decay slowly for $\alpha_2 > 1$. In figure (6*a*, *b*) the corresponding pressure profiles are shown for a large compression ratio $k = 10$. A qualitatively similar behaviour is observed except that in both figures there is a pronounced shift of the pressure maximum towards the trailing edge at $x = 0$ for case (*a*) and the leading edge at $x = 1$ for case (*b*). Note the six-fold difference in scales between figures 6(*a*) and 6(*b*) where the results for $\alpha = 0$ are the same, but mirror images of one another. In view of the large pressure gradients near the leading and trailing edges observed for large values of k one needs to be concerned about the assumption that the pressure is a constant across the porous layer in these regions. The length of these regions is of order H, whereas the length scale of the region with the steep pressure gradient is of order $1/k$. Thus, for the vertical pressure gradient

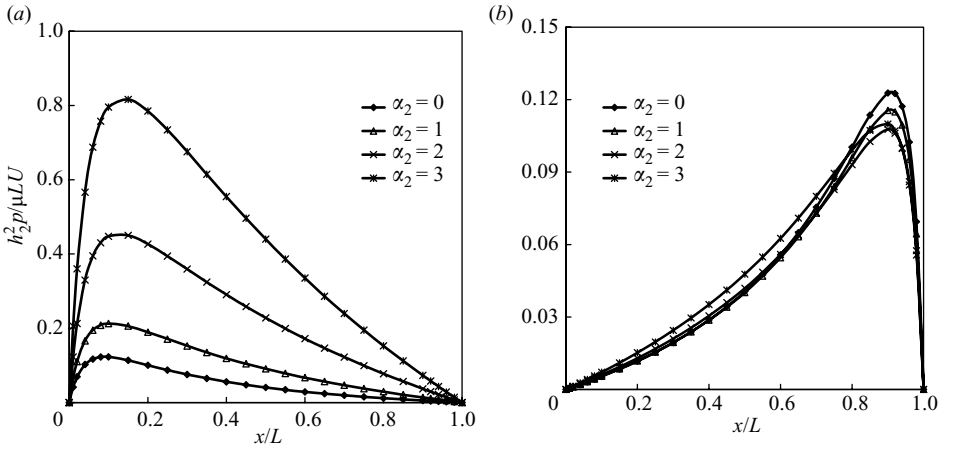

FIGURE 6. Dimensionless pressure distribution for compression ratio $k = 10$. (*a*) As the upper boundary moves and (*b*) as the lower boundary moves.

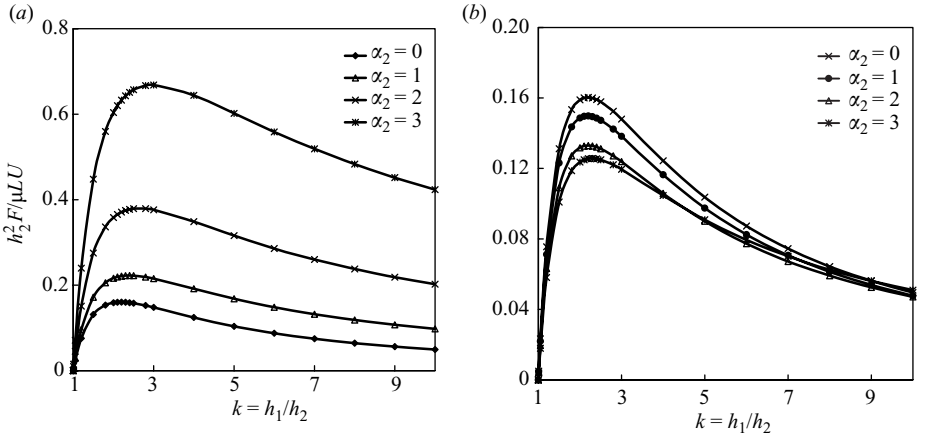

FIGURE 7. Dimensionless lift force as a function of compression ratio k. (*a*) Inclined upper boundary moves and (*b*) horizontal lower boundary moves.

to be neglected at the leading and trailing edges, we require $L/H > k$. The same approximation also applies for the classical lubrication results depicted in figure 4.

Figure 7 shows the dimensionless lift force as a function of k. We note that in figure 7(*a*) there is an optimum compression ratio for the dimensionless force at $k = 2.2$ when $\alpha = 0$, but when α increases its maximum increases in magnitude and shifts to values of $k > 2.2$. In case (*b*) (figure 7*b*), there is the same maximum at $k = 2.2$ when $\alpha = 0$, but the maximum decreases with increasing α. To examine the asymptotic behaviour for large α_2 we have rescaled the dimensionless pressure by α_2^2 in (4.14*a*) for case (*a*), since our asymptotic analysis in § 4.2 indicates that for case (*a*) the pressure and hence the lift force increases as α_2^2 increases. The analysis indicates that with this new scaling the new dimensionless pressure and lift force curves collapse into a single curve for large α_2. The results shown in figure 8(*a*) clearly indicate that there is very little difference between the curves for $\alpha_2 = 20$ and 100 and, thus, for most practical purposes the simplified asymptotic solution can be applied for $\alpha_2 > 20$. In contrast,

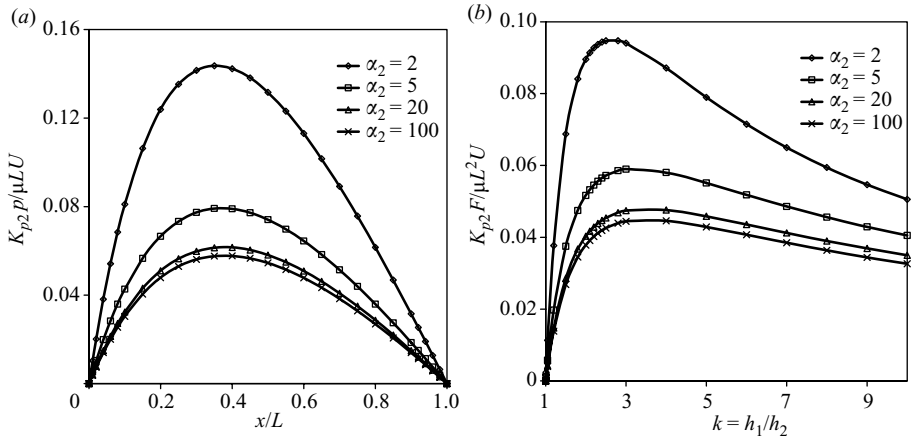

FIGURE 8. Asymptotic behaviour ($\alpha_2 \gg 1$) for pressure distribution. $k = 2$ (a) and lift force (b) when the inclined upper boundary moves (case a).

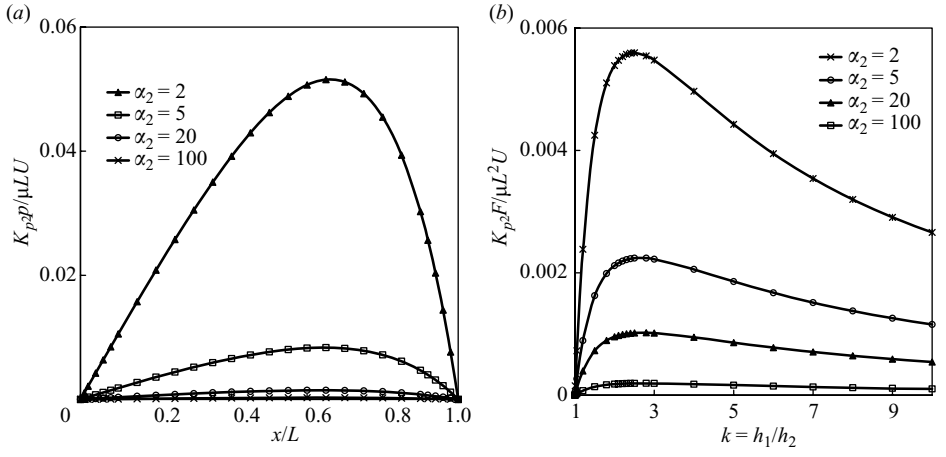

FIGURE 9. Asymptotic behaviour ($\alpha_2 \gg 1$) for pressure distribution. $k = 2$ (a) and lift force (b) when the horizontal lower boundary moves (case b).

the pressure disturbance and lift force for case (b), lower boundary moving, die out rapidly for $\alpha_2 \gg 1$, as shown in figure (9a, b).

Figures 10(a, b) show the velocity profiles in the fibre matrix for representative α_2 for cases (a) and (b), respectively, for $k = 4$. Three sets of profiles are shown in each panel, which corresponds to the leading and trailing edges and the position where the pressure reaches its maximum. For comparison the prediction of classical lubrication theory, $\alpha = 0$, is also shown. We note that at the position where the pressure gradient is zero in classical lubrication theory the velocity profile is linear, but as the fibre interaction layer parameter α_2 increases, thin fibre interaction layers develop near both the upper and lower boundaries provided there is a non-vanishing bulk flow in the matrix. In marked contrast to classical lubrication theory, where there is a uniform shear flow at the maximum pressure, it is the bulk flow that vanishes at the location where $\mathrm{d}p/\mathrm{d}x = 0$ for large α_2, since the local pressure gradient is the driving force for

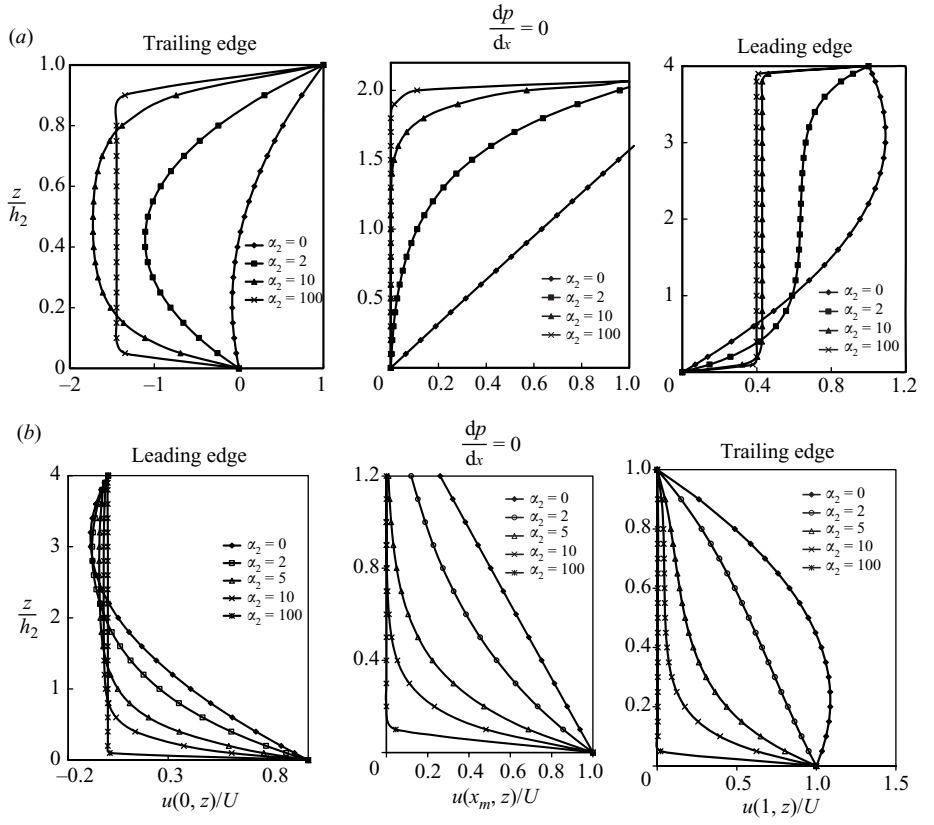

FIGURE 10. (*a*) Velocity profiles in fibre layer for representative α_2 when the upper boundary moves in the transformed steady coordinate frame where the upper boundary is stationary and the lower boundary with attached fibre layer moves beneath it, case (*a*). (*b*) Velocity profiles in fibre layer for representative α_2 when the lower boundary moves, case (*b*). Three sets of profiles are shown which correspond to the leading and trailing edges and the position where the pressure reaches its maximum, x_m ($k = 4$ for all profiles).

the flow in the interior of the fibre layer in this limit and this gradient vanishes at the maximum pressure. When there is no bulk flow, $u = -1$, since this is the velocity at which the fibre layer is moving to the left in the steady frame. In case (*b*), where the lower boundary is moving, an increasingly smaller amount of fluid is dragged through the leading edge as α_2 is increased since the fibre interaction layer near the lower boundary grows thinner and the bulk motion in the interior dies out for $\alpha_2 \gg 1$. In sharp contrast to classical lubrication theory, where the motion of lower boundary is transmitted as a shear force at the upper boundary, the presence of the fibre layer shields the upper boundary and serves as a barrier to greatly retard the flow. In case (*a*), large pressure gradients are generated in the interior of the fibre layer as α_2 increases. Basically, the inclined upper boundary is pushing fluid ahead of it in the unsteady reference frame in figure 1(*a*) creating a bulk flow in the fibre layer, which would vanish if this plane was not sloped upward. A curious feature for case (*a*), first pointed out in Feng & Weinbaum (2000), is that in the unsteady reference frame this flow is leaving at both the leading and trailing edges and a dividing streamline

develops beneath the inclined plane whose location depends on the compression ratio k.

6. Discussion

It may seem counter-intuitive, at first, that the solutions for cases (a) and (b) herein should differ so greatly from those of classical lubrication theory for a slider bearing when α is increased. However, the presence of the porous medium introduced an additional α^2 term in (2.3) when a steady-velocity transformation was introduced. The governing equation (2.3) thus differed depending on whether the porous media layer was attached to the lower or upper boundary. In marked contrast, in classical lubrication theory a simple transformation of coordinates leads to the same boundary value problem. Also, the numerical solutions in Feng & Weinbaum (2000) exhibit a lift force that monotonically increases with increasing k and the reason for the loss of the maximum at $k = 2.2$ was not clear. This result is now clearly explained by the results in figures 7(a) and 8(b) in which h_2, the height of the trailing edge in case (a) is fixed rather than h_1 at the leading edge. One observes there is an optimum compression ratio for the dimensionless force at $k = 2.2$ when $\alpha = 0$, but when α increases the maximum increases in magnitude and shifts to values of $k > 2.2$. This maximum is also present when the lower boundary is moving, but decays as α_2^2 for large α_2 as shown in figure 9(b).

The results in figures 8 and 9 provide the key insight into the difference in behaviour between red cells moving in single file in small capillaries and narrow glass tubes of the same diameter, as described in § 1. The value of α has been estimated as 160 for a 0.5 μm thick endothelial glycocalyx layer in Feng & Weinbaum (2000). The results in figure 8(a, b) show that for this value of α one has approached the limiting behaviour for both the pressure and the lift force exerted on the red cell membrane. Greatly enhanced lift forces separating the red cell and endothelial cell membranes will be present at very low velocities. These forces are more than four orders of magnitude greater than classical lubrication theory without the fibre layer present. Thus, the red cell will be displaced from the capillary wall when it is moving only a few micrometres per second, a speed which is much less than the $\sim$100 μm s^{-1} velocity that the red cell typically experiences in single-file flow in skeletal-muscle capillaries. This lift force is very important at arteriolar sphincters which control the distribution of flow in capillary networks. At these sphincters the vessels can narrow to as little as 4–5 μm diameter and the velocity of the red cell will slow to a few micrometres per second. The lift forces described herein prevent the glycocalyx from being crushed and the formation of adhesive interactions between membrane proteins in the red cell and the endothelial membranes that could lead to the arrest of the microcirculation. The behaviour of red cells in glass tubes suggested by the pressure profile in figure 9 is strikingly different. In this case the glycocalyx layer on the red cell membrane, whose existence has been hypothesized but not yet clearly demonstrated, generates a lift force that is nearly entirely attenuated for $\alpha > 20$. Therefore, tightly fitting red cells fill nearly the entire glass tube and experience much less resistance than red cells moving in capillaries with the same diameter as described by Pries *et al.* (1994, 2000).

The most important new result is the demonstration that the dimensionless lift force per unit width $(h_2^2 F)/(\alpha_2^2 \mu L^2 U)$, which can also be written as $(K_{p_2} F)/(\mu L^2 U)$, approaches a simple asymptotic behaviour for large α_2 as shown in figure 8(b). This result has important implications for generating lift forces on inclined surfaces moving over a stationary porous medium that vastly exceed those of classical lubrication

theory provided leakage of pressure at lateral edges can be eliminated. This was realized in F&W and Wu *et al.* (2004), but an inexpensive soft durable fibrous material had not yet been identified. The properties of such a material are explored in Mirbod *et al.* (in press). This material is a random fibre matrix with nearly uniform 10 μm diameter polyester fibres with a trace of silk. K_p for these fibres is well described by an empirical Carman–Kozeny relation for porous media. The experiments in Mirbod *et al.* (in press) show that the length of fibre per unit volume is 5950 cm cm^{-3} in its undeformed state. This corresponds to a solid fraction of 0.0045 and a value of K_p of 3.4×10^{-5} cm^2 using figure 2. It is a simple matter to calculate the lift force on a planing surface for any value of the compression ratio k using figure 8(*b*). As a practical matter a light highly porous protective screen rests on top of the porous layer. This is tethered to the impermeable sidewalls of the channel to reduce shear deformation.

To illustrate the above application consider a planform with the typical dimensions of a toboggan, 2 m long and 0.5 m wide or a planning area of 1 m^2. Assume that h_1 at the leading edge is 10 cm and h_2 at the trailing edge is 5 cm or $k = 2$. If the layer compresses in a locally uniform manner the solid fraction at the trailing edge will be doubled or $(1 - \varepsilon) = 0.009$. From figure 2, $K_{p_2} = 1.57 \times 10^{-9}$ m^2 and $\alpha_2 = 1260$. The curve for $(K_{p_2}F)/(\mu L^2 U)$ for $\alpha_2 = 1260$ is nearly indistinguishable from the curve for $\alpha_2 = 100$ in figure 8(*b*). For $k = 2$, $(K_{p2}F)/(\mu L^2 U)$ is 0.037. All the parameters in the dimensionless expression for the lift force are now known except for U, but the latter scaling is linear. Using the value of μ for air at 20 °C, which is 1.73×10^{-5} Ns m^{-1}, one finds that $F = 815\,U$ in Nm s^{-1}. At a velocity of 10 m s^{-1} this toboggan can support 8150 N or 0.83 metric tons. This force due to the trapped air in the porous material is many times the lift force of the solid phase because the material has the softness of cotton. It is hard to imagine that so much weight can be supported by a material with the properties of a common pillow with relatively little compression.

As first proposed in Wu *et al.* (2004) such large lift forces could potentially be used in commercial transportation. In Mirbod *et al.* (in press), we explore this concept for a 200 passenger jet train weighing approximately 70 metric tons, supported by a 30×3 m planform that glides on a 20 cm thick soft porous track in a channel a few tens of centimetres above the surface of the ground. The calculations in Mirbod *et al.* (in press) predict that the train would become airborne at velocities less than 5 m s^{-1} with only a 20 % compression of the fibre layer (4 cm) at the trailing edge of the planform for lift-off. For a 10 μm fibre the Reynolds number (Re) at lift off is ~0.5. For such small compressions the fibre phase provides less than 0.5 % of the total lift and friction forces are negligible compared to aerodynamic drag. The track requires a highly porous light-weight protective screen that rests on the top of the porous layer to protect it from wear, tear and debris. This protective screen could also have narrow felt gliding strips at its edges to minimize pressure leakage at the lateral edges of the planform. It would also greatly reduce shear deformation in the thin fibre interaction boundary layer beneath the moving inclined upper boundary. One finds that this airborne jet train needs far less powerful jet engines and consumes far less energy than commercial aircraft with the same passenger load since there is no need to climb to cruising altitude and lift induced drag is negligible since the maximum angle of attack is less than 0.1 °.

The authors acknowledge the financial support by NSF grant no. 0432229. This research was completed in partial fulfillment of the requirements for the PhD degree of Parisa Mirbod from The City College and the City University of New York.

REFERENCES

Brinkman, H. C. 1947 A calculation of the viscous force exerted by a flowing fluid in a dense swarm of particles. *Appl. Sci. Res.* A **1**, 27–34.

Chien, S., Usami, S. & Skalak, R. 1984 Blood flow in small tubes. In *Handbook of Physiology, Circulation. Section on Microcirculation* (ed. E. M. Renkin & C. Michel), pp. 217–249. American Physiological Society.

Damiano, E. R. 1998 The effect of the endothelial-cell glycocalyx on the motion of red blood cells through capillaries. *Microvasc. Res.* **55**, 77–91.

Damiano, E. R. & Stace, T. M. 2002 A mechano-electrochemical model of radial deformation of the capillary glycocalyx. *Biophys. J.* **82**, 1153–1175.

Feng, J. & Weinbaum, S. 2000 Lubrication theory in highly compressible porous media: the mechanics of skiing, from red cells to humans. *J. Fluid Mech.* **422**, 288–317.

Han, Y., Ganatos, P. & Weinbaum, S. 2005 Transmission of steady and oscillatory fluid shear stress across epithelial and endothelial surface layers. *Phys. Fluids* **17**, 031508(1–13).

Han, Y., Weinbaum, S., Spaan, J. A. E. & Vink, H. 2006 Large-deformation analysis of the elastic recoil of fibre layers in a Brinkman medium with application to the endothelial glycocalyx. *J. Fluid Mech.* **554**, 217–235.

Happel, J. & Brenner, H. 1983 *Low Reynolds Number Hydrodynamics: With Special Applications to Particulate Media.* Springer.

Mirbod, P., Andreopoulos, Y. & Weinbaum, S. An airborne jet train that flies on a soft porous track. *Proc. Natl. Acad. Sci.* in press.

Pries, A. R., Secomb, T. W. & Gaehtgens, P. 2000 The endothelial surface layer. *Pflugers Arch.* **440**, 653–666.

Pries, A. R., Secomb, T. W., Gessner, T., Sperandio, M. B., Gross, J. F. & Gaehtgens, P. 1994 Resistance to blood flow in microvessels in vivo. *Circ. Res.* **75**, 904–915.

Roy, B. C. & Damiano, E. R. 2008 On the motion of a porous sphere in a Stokes flow parallel to a planar confining boundary. *J. Fluid Mech.* **606**, 75–104.

Sangani, A. S. & Acrivos, A. 1982 Slow flow past periodic arrays of cylinders with application to heat transfer. *Intl J. Multiphase Flow* **8**, 193–206.

Schlichting, H. 1979 *Boundary Layer Theory*, sixth edn. McGraw-Hill.

Secomb, T. W., Hsu, R. & Pries, A. R. 1998 A model for red blood cell motion in glycocalyx-lined capillaries. *Am. J. Physiol. Heart Ciric. Physiol.* **274**, H1016–H1022.

Secomb, T. W., Hsu, R. & Pries, A. R. 2001 Motion of red blood cells in a capillary with an endothelial surface layer: effect of flow velocity. *Am. J. Physiol. Heart Circ. Physiol.* **281**, H629–H636.

Thi, M. M., Tarbell, J. M., Weinbaum, S. & Spray, C. D. 2004 The role of the glycocalyx in reorganization of the actin cytoskeleton under fluid shear stress: A "bumper-car" model. *Proc. Natl. Acad. Sci.* **101**, 16483–16488.

Truskey, G. A., Yuan, F. & Katz, D. F. 2004 *Transport Phenomena in Biological Systems.* Prentice Hall.

Vink, H. & Duling, B. R. 1996 Identification of distinct luminal domains for macromolecules, erythrocytes and leukocytes within mammalian capillaries. *Circ. Res.* **71**, 581–589.

Weinbaum, S., Tarbell, J. M. & Damiano, E. R. 2007 The structure and function of the endothelial glycocalyx layer. *Annu. Rev. Biomed. Eng.* **9**, 121–167.

Weinbaum, S., Zhang, X., Han, Y., Vink, H. & Cowin, S. 2003 Mechanotransduction and flow across the endothelial glycocalyx. *Proc. Natl. Acad. Sci.* **100**, 7988–7996.

Wu, Q., Andreopolous, Y. & Weinbaum, S. 2004 From red cells to snowboarding: a new concept for a train track. *Phys. Rev. Lett.* **93** (19), 194501.

Wu, Q., Andreopoloulos, Y., Xanthos, S. & Weinbaum, S. 2005 Dynamic compression of highly compressible porous media with application to snow compaction. *J. Fluid Mech.* **542**, 281–304.

Wu, Q., Igci, Y., Andreopoulos, Y. & Weinbaum, S. 2006 Lift mechanics of downhill skiing and snowboarding. *Med. Sci. Sports Exer.* **38** (6), 1132–1146.